Trapping Light, Tracking Proteins: Enhancing Time Resolution for Electron Paramagnetic Resonance Spectroscopy Studies of Protein Motion Using Fabry-Pérot Capillaries

Seda Peacher, Johanna Schubert and Mark Sherwin
Sherwin Group, Department of Physics, University of California, Santa Barbara, Broida Hall, Santa Barbara, CA 93106

Understanding protein motion is essential to elucidating protein biological function. However, capturing protein dynamics in real time remains challenging due to small molecular size and rapid timescales of motion involved. Sherwin Lab employs time-resolved rapid-scan electron paramagnetic resonance spectroscopy with Gadolinium-3+ spin labels (rs-TiGGER) to track changes in distance between labeled protein sites in real time. Currently, the temporal resolution for this technique is limited to about 10 ms. To enable detection of faster dynamics, we attempt to enhance signal-to-noise ratio via the development of Fabry–Pérot cavity-like sample capillaries. To form semireflective surfaces for Fabry–Pérot interference, the rectangular borosilicate glass capillaries are coated are coated in indium tin oxide (ITO). We evaluate cavity performance by simulating ITO-deposited capillaries filled with air, water, and a custom protein buffer solution (20 mM Tris-HCl, 150 mM NaCl, pH 7.50) to mimic a functional setup that can then be fabricated. We determined the refractive index of the borosilicate glass, modeled the behavior of water and buffer solutions within the capillary, and simulated the optical response of ITO using the transfer matrix method. The simulations suggest that the initially planned design does not produce Fabry–Pérot resonance. Therefore, moving forward, we plan to use well-plate geometry to gain the desired result.

I. INTRODUCTION

A. Protein Background and Motion

Proteins are essential building blocks of life and perform a remarkable variety of functions in all living organisms. The Protein Data Bank is a scientific resource containing over 200,000 protein structures cataloged using traditional methods suited for static protein analysis.[2] Recently, the Protein Data Bank played a key role in training AlphaFold, a groundbreaking AI tool developed by Google DeepMind that was recognized with the Nobel Prize in Chemistry. AlphaFold can predict the 3D structure of a protein from its linear sequence of amino acid residues, which determine the primary level of protein structure.[2]

The cataloging of static proteins and the generation of 3D protein structures represent current state-of-the-art protein research. Although this is a remarkable achievement, understanding protein function requires more than just static snapshots, as many proteins rely on movement and conformational changes to perform their function. The development of techniques to film protein motion in real time is the cutting edge of modern protein research.

B. Electron Paramagnetic Resonance Spectroscopy Theory

Sherwin Group combines rapid scan electron paramagnetic resonance (rs-EPR) spectroscopy and site-directed spin labeling to "film" protein in motion. EPR takes advantage of the quantum mechanical behavior of materials that have unpaired electrons. Electron spins can exist in one of two states: spin-up or spin-down. In EPR spectroscopy, the magnetic field is swept through a resonant value that corresponds to the energy difference between electron spin states, which is set by the microwave frequency. Due to the Maxwell–Boltzmann distribution, more electrons naturally occupy the lower-energy (spin-down) state than the higher-energy (spin-up) state at thermal equilibrium. As the magnetic field approaches the resonant value, the energy difference between these spin states matches the energy of the applied microwaves, allowing transitions from the lower to the higher state. This imbalance in population enables the net absorption of energy, which forms the basis of the EPR signal.[6] The resulting EPR spectrum can then be analyzed to extract information about molecular structure and spatial arrangement.

Sherwin Lab uses a specific type of EPR called rapid-scan electron paramagnetic resonance (rs-EPR), in which the magnetic field is swept rapidly back and forth through resonance. Unlike conventional continuous-wave EPR, which records the signal point-by-point as the field is slowly varied, rs-EPR repeatedly captures the entire spectrum in a single, rapid scan. This approach greatly improves time resolution, allowing dynamic processes to be followed on much shorter timescales. It also enhances the signal-to-noise ratio by effectively averaging over many rapid passages through resonance. Gadolinium spin labels are used because they create a sharp, narrow linewidth during EPR spectroscopy, are not sensitive to chemical environment.

C. EPR for "Filming" Protein Motion

Proteins generally do not contain unpaired electrons, so paramagnetic spin labels with unpaired electrons must be introduced at specific sites within the protein. Since EPR lineshape depends on the distance between these spin labels, the sites must be specially chosen to provide information on the movement of proteins.

Sherwin Lab has used rs-TiGGER on AsLOV2, or the Light-Oxygen-Voltage (LOV)2 domain of *Avena sativa* (oat) phototropin 1. When activated with a 450 nm blue laser, the Jα-helix unfolds in under 1ms and then refolds on a minute timescale. As depicted in Figure 1, the distance between the spin labels attached to the proteins changes as the helix unfolds and refolds, which results in a change in the EPR spectrum in real time. We can then create a graph of the changes over time in the linewidth of this spectra, and we fit that graph to see the recovery timescale.[4]

So far, this technique has only worked for the refolding of the helix. Our current time ceiling is around 10 ms, meaning that we cannot capture the unfolding yet. The unfolding occurs on a timescale similar to that of other biologically relevant protein behaviors, making it all the more relevant to develop a tool that would allow us to track these rapid protein motions.

D. Physics of Fabry-Pérot Signal Enhancement

Improving signal-to-noise ratio increases time resolution because once the signal stands out clearly from the noise, it can be measured more accurately over shorter time intervals, preserving fine temporal structure instead of averaging it away. One strategy for trying to increase signal to noise ratio and therefore improve the time ceiling is to add a resonator. Many EPR labs already function with a resonator, as the EPR signal is relatively weak, especially at low fields. Sherwin Lab operates at very high fields and a resonator has not been critical up to this point.

We have chosen to use a Fabry–Pérot resonator, or an optical system composed of two reflective surfaces positioned at a precise distance from each other. The resonator, or cavity, confines electromagnetic waves between partially reflecting boundaries, allowing only wavelengths that constructively interfere to form standing waves within the cavity. This resonance greatly enhances the field intensity in the sample region, improving sensitivity for spectroscopic measurements, which in our case, is the detection of proteins.[3] (See Fig. 2). To create the cavity, indium tin oxide (ITO) was deposited onto rectangular borosilicate glass capillaries. (See Fig 3).

II. METHODS AND RESULTS

A. Vector Network Analyzer Measurements of Borosilicate Glass Capillary

A Vector Network Analyzer (VNA) was used to analyze the optical properties of the sample capillaries in a frequency range relevant for the protein measurements. The VNA measured the S11 parameter, or the reflective parameter. By analyzing S11, the VNA helps determine the cavity's resonant frequency and quality (Q) factor, which is the ratio of the initial energy stored in the cavity to the energy lost per cycle of oscillation.

The area measurements are taken over is too large for a singular capillary, so three capillaries had to be set next to each other to obtain accurate data. In order to keep the angle constant and hold the three capillaries together, an angle jig that fits exactly 3 capillaries was designed in CAD and 3D printed. (See Fig. 4)

To verify capillary angle does not affect the measurement, the VNA measured the same part of capillaries while the angle in the jig was changed. The results suggested that angle does not affect the position of the minimum or the magnitude, and will not need to be considered in the sample exchange design. (See Fig. 5).

However, as different locations along the length of one capillary are measured, the position of the minimum is shifted, and the index of refraction is different when fit. (See Fig. 6). This means that the thickness of the glass must be variable along the capillary. This presents an experimental challenge, because we have to tune the thickness of the ITO to get Fabry–Pérot resonance, and if the glass thickness is variable, then the ITO deposition thickness would need to be different every time.

B. Transfer Matrix Method Modeling

The Transfer Matrix Method (TMM) was used to model the empty capillaries and extract the refractive index of the borosilicate glass. TMM consists of characterizing each material and interface with matrices I and P respectively.

$$M = I_{01} \cdot P_1 \cdot I_{12} \cdot P_2 \cdot I_{23} \cdot P_3 \cdot I_{34} \cdot P_4 \cdot I_{45} \cdot P_5 \cdot I_{56} \quad (1)$$

These matrices are multiplied together to obtain a global transfer matrix:

$$r(f) = \frac{M_{21}}{M_{11}}, \quad (2)$$

and then converted to decibels to be able to be fit over the VNA measurements:

$$S_{11}(f) = 20 \log_{10} |r(f)|. \quad (3)$$

I used the transfer matrix method above to fit the refractive index of glass, allowing it to be complex because

borosilicate glass is not perfectly lossless and absorbs some of the incoming light. (See Fig. 7). Once I had the refractive index of the glass, we could start to work with filled capillaries.

When protein measurements are taken, the capillaries will be filled with a liquid buffer. We started by modeling water, which is a bit simpler. The same model used for modeling the empty capillaries did not work well on the water filled capillaries. We hypothesize that this is because water is lossy in THz to GHz range and more factors need to be considered in light of that.

Using a form of the complex dielectric function allows for the additional factors needed. This equation is the complex dielectric function in its simplest form:

$$\epsilon^*(\nu) = \epsilon'(\nu) + i\epsilon''(\nu). \tag{4}$$

The function itself quantifies how a material responds to an electric field with a certain frequency. It has a real part, ϵ', related to the storage of electrical energy within the material, and an imaginary part, ϵ'', related to the dissipation of energy by the material, whether it is through absorption or scattering.

This function can also be written in terms of Debye relaxations, which describe how fast molecules respond to changes in an electric field, especially when the field is changing rapidly, like in terahertz radiation:

$$\epsilon^* = \epsilon_\infty + \sum_{j=1}^{n} \frac{\Delta\epsilon_j}{1 + i2\pi\nu\tau_j}.^7 \tag{5}$$

This expansion is for particulates in some medium, or a solution. In this equation, ϵ_∞ is the permittivity at the high frequency limit, $\Delta\epsilon$ is the weighted contribution of each Debye process to the total relaxation, τ is the relaxation time of each Debye process, and ν is the frequency of the incoming radiation. The complex index of refraction is the square root of the complex dielectric function,

$$\epsilon(\nu) = N(\nu)^2 = (n(\nu) - ik(\nu))^2, \tag{6}$$

so we can use our results to create a more accurate simulation of the water filled capillary using that index of refraction we get and the transfer matrix method. (See Fig. 8).

The buffer is is 20 mM Tris-HCl and 150 mM NaCl with a pH of 7.50. Salt binds to the extra charges on parts of the protein that could lead to unexpected motion. Modeling the buffer incorporates the same equation as the water, just with an added ionic conductivity term to account for the presence of salt:

$$\epsilon^* = \epsilon_\infty + \sum_{j=1}^{n} \frac{\Delta\epsilon_j}{1 + i2\pi\nu\tau_j} + \frac{\sigma}{2\pi\nu\epsilon_0}.^7 \tag{7}$$

In comparing figures 8 and 9, it is evidence that the buffer does not differ much from water. The buffer is pH 7.5, and only has 150 mM of salt added, so this is in line with our predictions.

The Drude Free Electron Model was used to calculate the refractive index of ITO.‘[1] This equation is Drude Free Electron model equation of motion for the average electron velocity in the presence of an electric field:

$$m\frac{dv}{dt} = -eE - \frac{mv}{\tau}. \tag{8}$$

Its frequency-domain solution is another rewriting of the complex dielectric function that models electrons in a metal as a gas of randomly-moving particles that do not interact with one another:

$$\epsilon(\omega) = \epsilon_\infty - \frac{\omega_P^2}{\omega^2 + \frac{i\omega}{\tau}}.^1 \tag{9}$$

This comes from applying classical equations of motion to electrons modeled as small balls in a sort of dense soup driven by an electric field. Here, ϵ_∞ is again the permittivity at the high frequency limit, and the second term arises from the free carriers for which τ is the momentum relaxation time, ω_P is the characteristic plasma frequency, and ω is the frequency of the field. Once we got this result using values from the literature, we were able to take the square root of this to get the complex index of refraction, and model the ITO.

In these simulation results, we are looking specifically at 240 GHz, because that is the frequency our EPR setup measures at, and we are looking for deep minima that are sharp, or have narrow linewidths. The minima should occur at 240GHz, because that means we have resonance where we are measuring, and they should be sharp because the narrower the linewidth the better the Q, or quality, factor. ITO is not very reflective in the sub 50 nm regime, so that is the thinnest the model can be applied to.[5]

Figure 10), does not posess any of the above qualities. There are wide minima, and more importantly no minimum at 240GHz, meaning there is no resonance there. Once the capillaries are filled, the location of the minima will shift because the optical length will change, but that is not the only issue.

Another contributing factor is hypothesized to be that the path of the light is more complicated than the initial Fabry–Pérot figure suggests. There are not just the two reflective layers, the glass layers and the core filling must also be accounted for. As the light is transmitted through the system, it is partially absorbed by and reflected off of each layer, causing more complicated wave interactions than were originally assumed.

In particular, one of the issues is hypothesized to be that in the initial light-ITO interaction, the interface is with air, but in the second interaction the interface is with glass. The ITO cannot be deposited on the inside to mitigate this issue, so the thickness of the second layer is varied instead.

Figure 11 depicts the result with the filled the capillary and varied the ITO deposition on the second layer. The

quality of the minima is better, and the location is much closer to the desired 240 GHz.

III. DISCUSSION

Unfortunately, while we might be able to see Fabry–Pérot like enhancement with the filled capillary and variable deposition on one side, we cannot create a true resonator, because there is not enough room within the capillary to create a standing wave for resonance. The capillaries have a 0.1mm core, but the wavelength of the EPR signal is 1.25mm.

Additionally, the capillaries cannot be reused, as they cannot be appropriately cleaned since they are so small, and the liquid inside evaporates quickly. This is a problem particularly because, due to the variable glass thickness, ITO deposition thickness would need to vary with every capillary, which would make experimental setup tedious and hard to keep consistent. In light of that, our next step is to create a model of a functional setup.

IV. CONCLUSIONS

We need to create more space between ITO layers to allow standing waves to form and resonance to occur at 240 GHz, and one of our options to do so is well plate geometry. (See Fig. 12). We will model this in python, as we have the previous experiments. Once we have a functional setup modeled, we will deposit the ITO using e-beam evaporation, which uses a focused beam of electrons to evaporate a material, in our case ITO, which then is deposited as a thin film on a substrate. After deposition, we will analyze the setup with the VNA to confirm agreement with the simulation results, and test the cavity with EPR spectroscopy.

Resolving fast protein motions remains difficult with existing techniques. A Fabry–Pérot cavity would enhance the signal to noise ratio, and improving signal to noise ratio increases time resolution because once the signal stands out clearly from the noise, it can be measured more accurately over shorter time intervals.

This increased signal to noise ratio and time ceiling would pave the way for Sherwin Lab and our EPR spectroscopy to resolve faster protein dynamics and track never before seen protein motion in real time.

V. ACKNOWLEDGEMENTS

This work is supported by NSF REU grant PHY-2349677. Thank you to the REU program director, Dr. Sathya Guruswamy, my faculty mentor, Dr. Mark Sherwin, my graduate student mentor, Johanna Schubert, staff scientists Qile Wu and Nick Agladze, and graduate students Alex Giovannone, Juan Gaitan, and Moonsuk Jang for their help and support throughout this summer.

[1] Chen, C.-W., Lin, Y.-C., Chang, C.-H., Yu, P., Shieh, J.-M., and Pan, C.-L. (2010). Frequency-Dependent Complex Conductivities and Dielectric Responses of Indium Tin Oxide Thin Films from the Visible to the Far-Infrared. *IEEE Journal of Quantum Electronics*, 46(12):1746–1754.

[2] Jumper, J., Evans, R., Pritzel, A., Green, T., Figurnov, M., Ronneberger, O., Tunyasuvunakool, K., Bates, R., Žídek, A., Potapenko, A., Bridgland, A., Meyer, C., Kohl, S. A. A., Ballard, A. J., Cowie, A., Romera-Paredes, B., Nikolov, S., Jain, R., Adler, J., Back, T., Petersen, S., Reiman, D., Clancy, E., Zielinski, M., Steinegger, M., Pacholska, M., Berghammer, T., Bodenstein, S., Silver, D., Vinyals, O., Senior, A. W., Kavukcuoglu, K., Kohli, P., and Hassabis, D. (2021). Highly accurate protein structure prediction with AlphaFold. *Nature*, 596(7873):583–589.

[3] Perot, A. and Fabry, C. (1899). On the Application of Interference Phenomena to the Solution of Various Problems of Spectroscopy and Metrology. *Astrophys. J.*, 9:87.

[4] Price, B. D., Sojka, A., Maity, S., Chavez, M. I., Stark, M., Wilson, M. Z., Han, S., and Sherwin, M. S. (2024). Field-domain rapid-scan EPR at 240GHz for studies of protein functional dynamics at room temperature. *Journal of Magnetic Resonance*, 366:107744.

[5] Saeed, U., Abdel-wahab, M., Sajith, V., Ansari, M., Ali, A. M., and Al-Turaif, H. (2019). Characterization of an amorphous indium tin oxide (ito) film on a polylactic acid (pla) substrate. *Bulletin of Materials Science*, 42.

[6] Toida, H., Matsuzaki, Y., Kakuyanagi, K., Zhu, X., Munro, W. J., Yamaguchi, H., and Saito, S. (2019). Electron paramagnetic resonance spectroscopy using a single artificial atom. *Communications Physics*, 2(1):33.

[7] Vinh, N. Q., Sherwin, M. S., Allen, S. J., George, D. K., Rahmani, A. J., and Plaxco, K. W. (2015). High-precision gigahertz-to-terahertz spectroscopy of aqueous salt solutions as a probe of the femtosecond-to-picosecond dynamics of liquid water. *The Journal of Chemical Physics*, 142(16):164502.

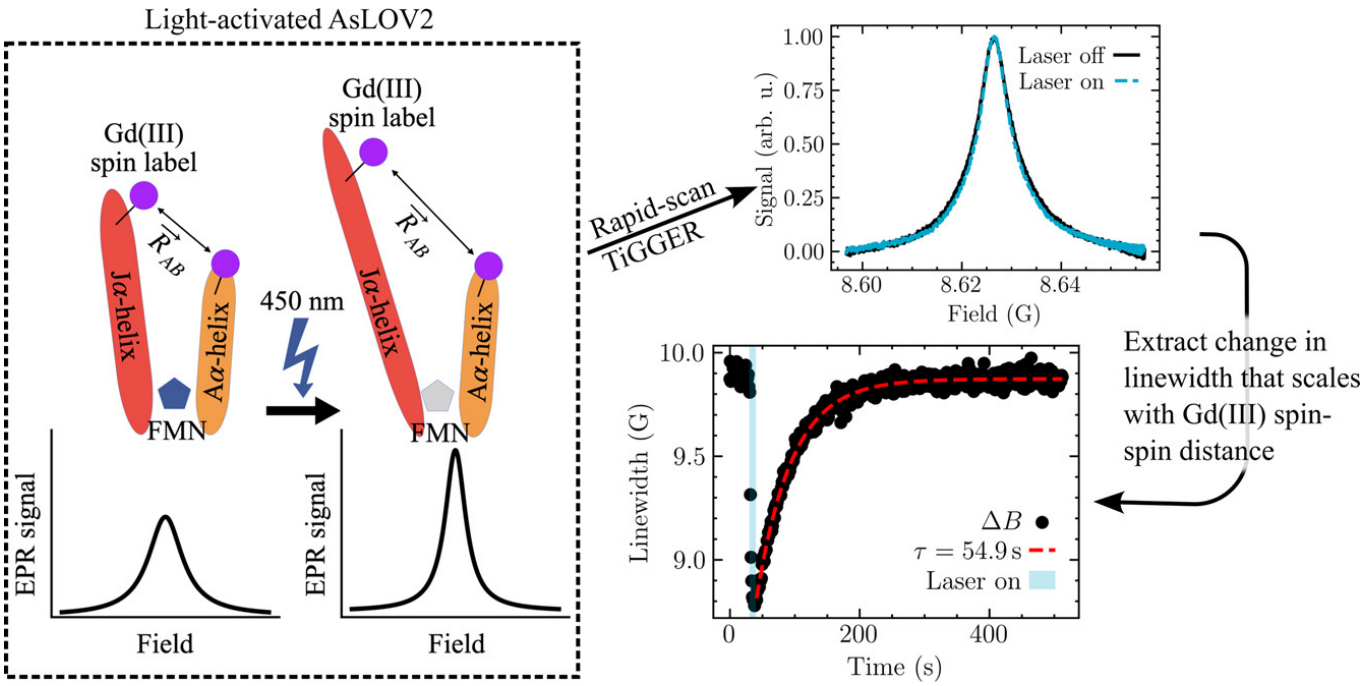

FIG. 1. Light-induced conformational changes in AsLOV2 monitored by Gd(III)–Gd(III) rapid-scan EPR spectroscopy. Upon 450 nm illumination, the relative orientation of the Jα-helix and Aα-helix changes, altering the Gd(III)–Gd(III) spin–spin distance (R_{AB}). This structural rearrangement modifies the EPR spectrum, observed as a light-dependent change in linewidth. Rapid-scan TiGGER analysis quantifies the linewidth broadening (ΔB), which directly scales with spin–spin distance, yielding a kinetic time constant ($\tau \approx 54.9$s) for the photoresponse.[4]

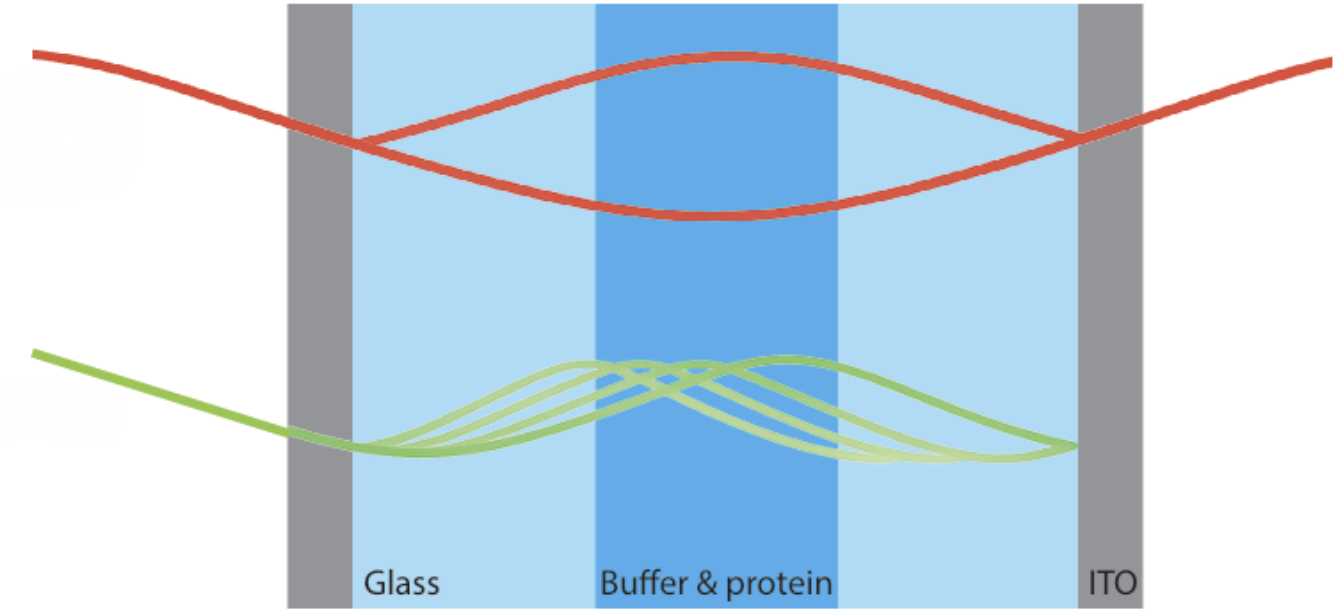

FIG. 2. Concept of Fabry–Pérot resonance.

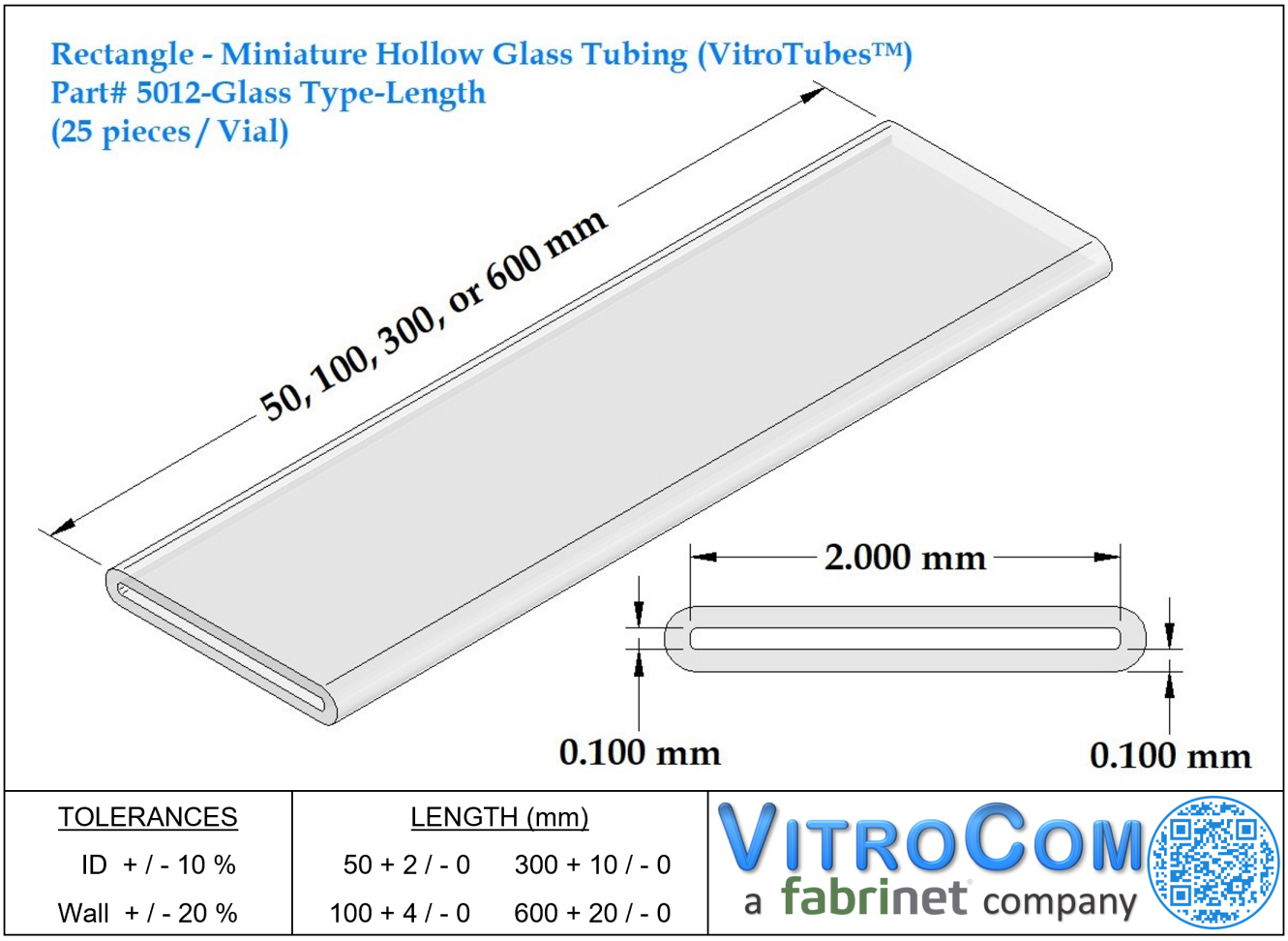

FIG. 3. VitroCom rectangular borosilicate glass capillaries were used in this study. To achieve the desired length for measurement, we broke each long capillary tube into roughly inch-long pieces.

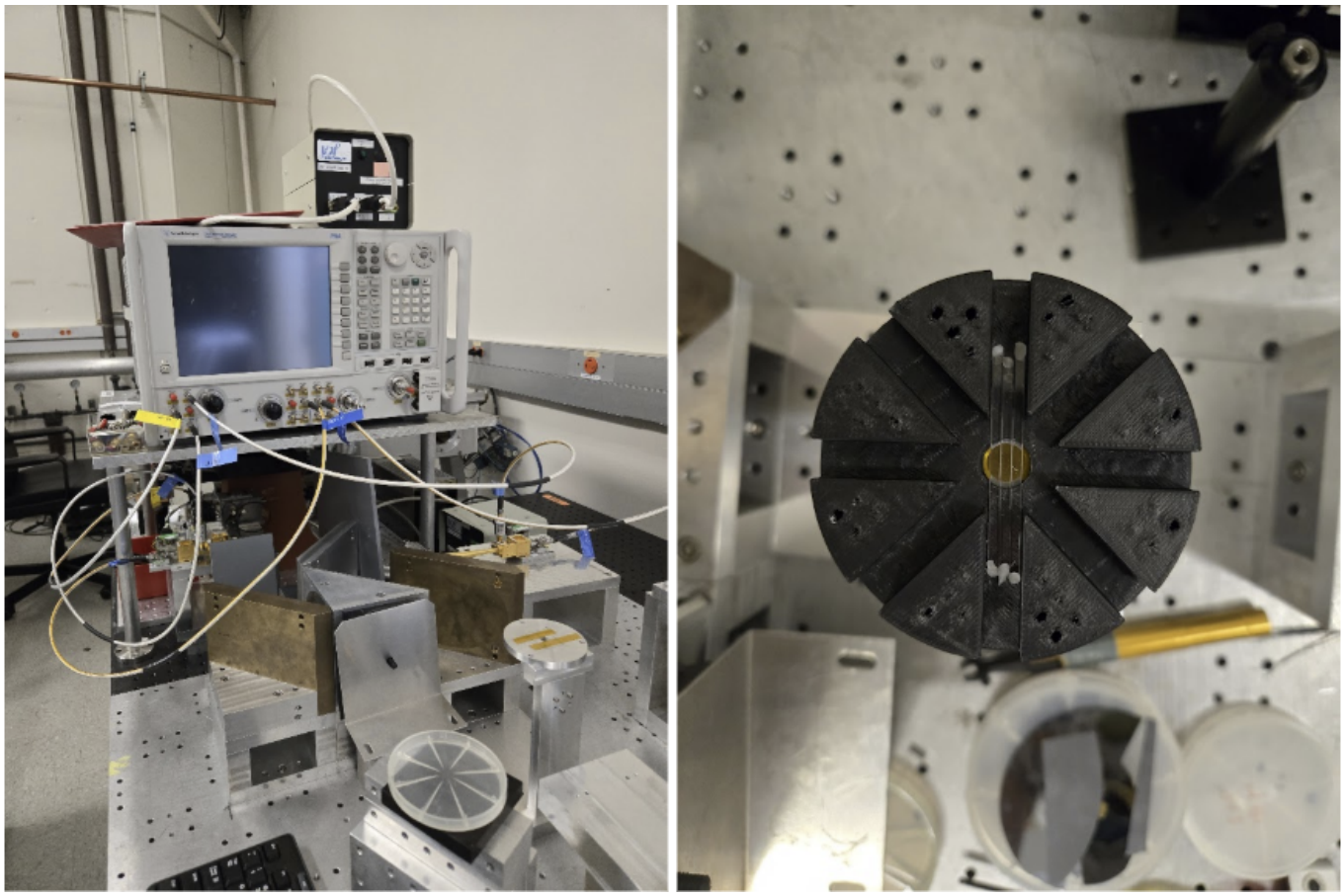

FIG. 4. Left: The VNA measurement setup. Right: Filled capillaries in 3D printed angle jig on sample stage.

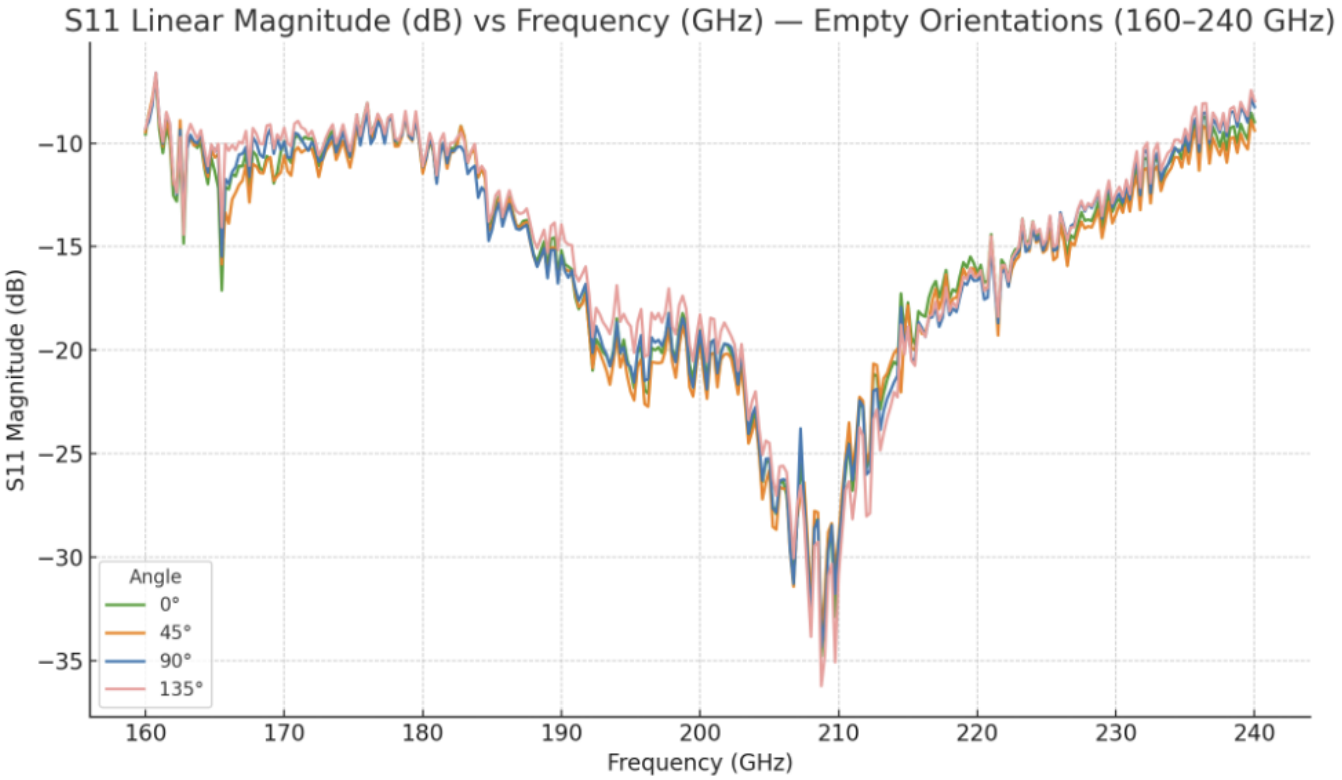

FIG. 5. Empty capillaries measured in varying positions on the angle jig. Due to the length of the capillaries, each angle on the graph also corresponds to its reference angle.

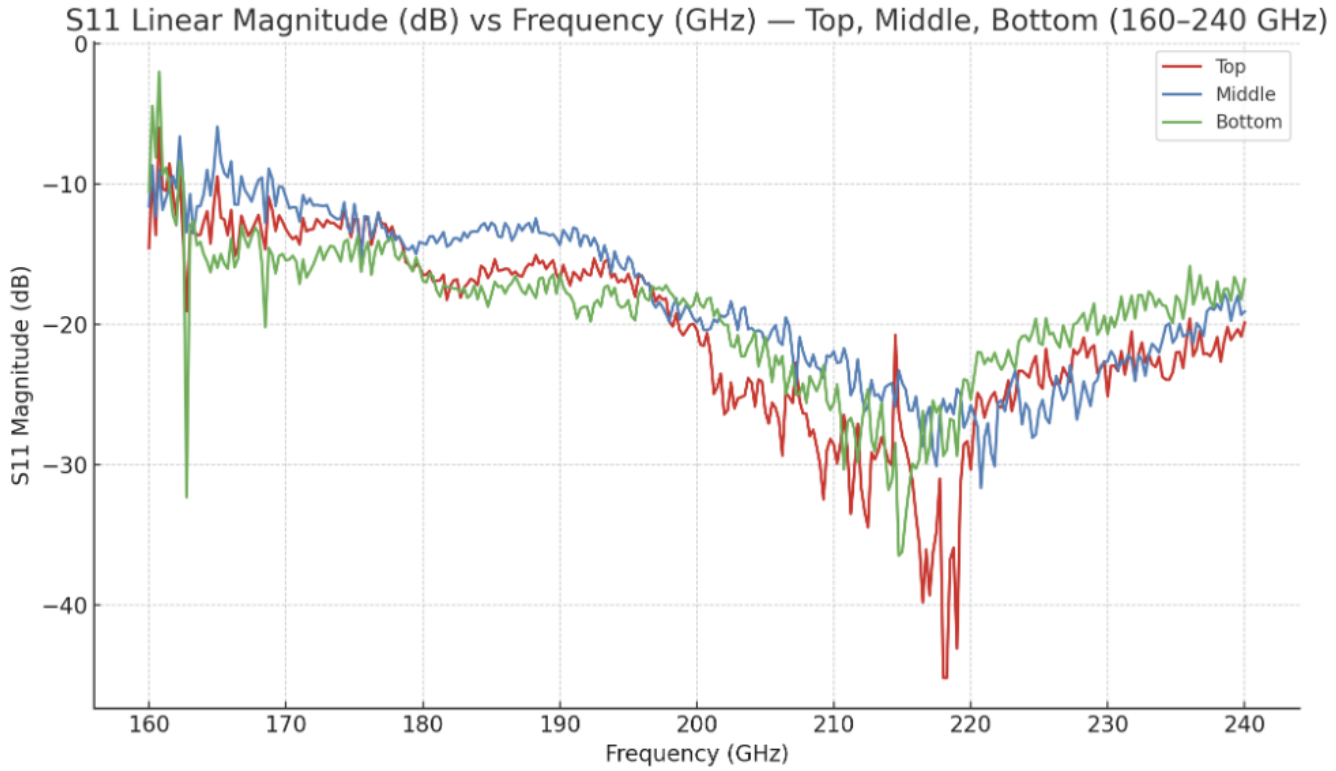

FIG. 6. Empty capillary measured along its length at a consistent angle.

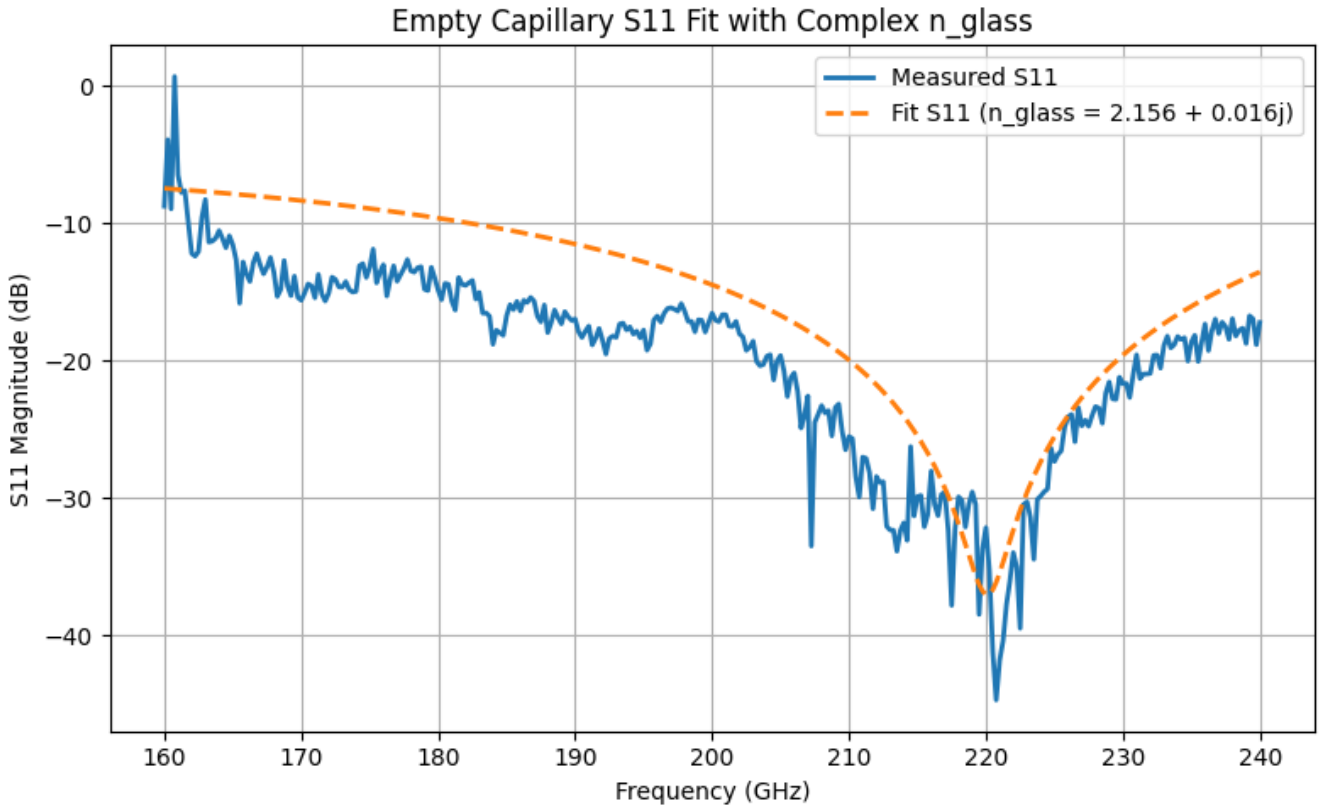

FIG. 7. S11 Magnitude (dB) vs. Frequency (GHz) for empty uncoated borosilicate glass capillaries.

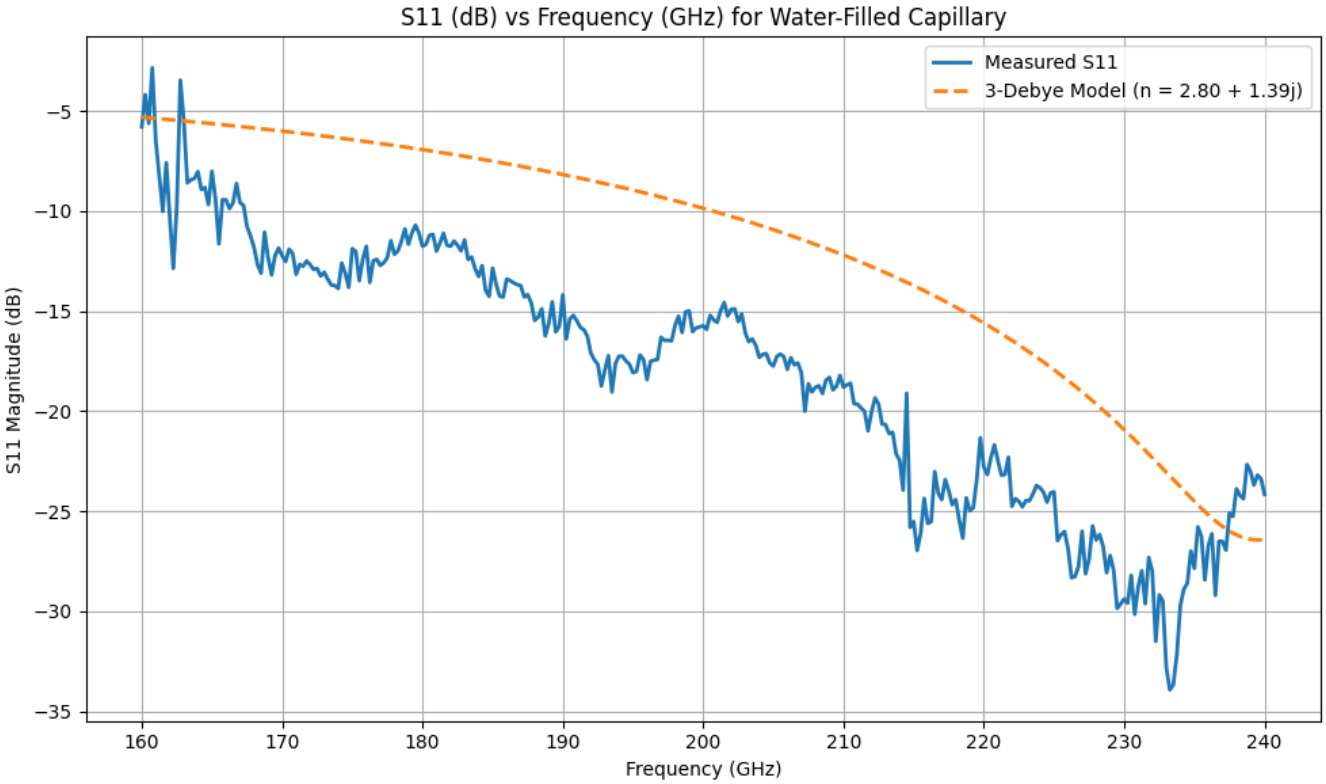

FIG. 8. S11 Magnitude (dB) vs. Frequency (GHz) for water-filled uncoated borosilicate glass capillaries.

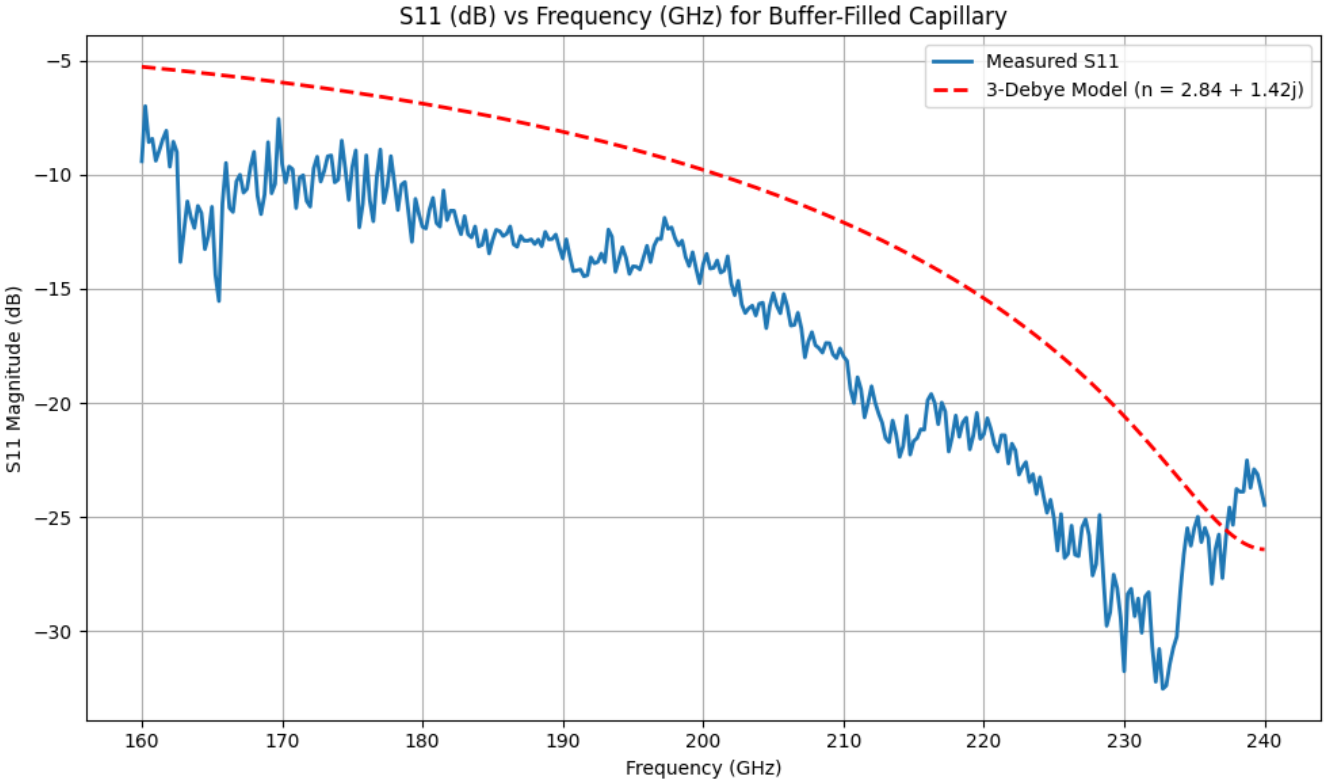

FIG. 9. S11 Magnitude (dB) vs. Frequency (GHz) for buffer-filled uncoated borosilicate glass capillaries.

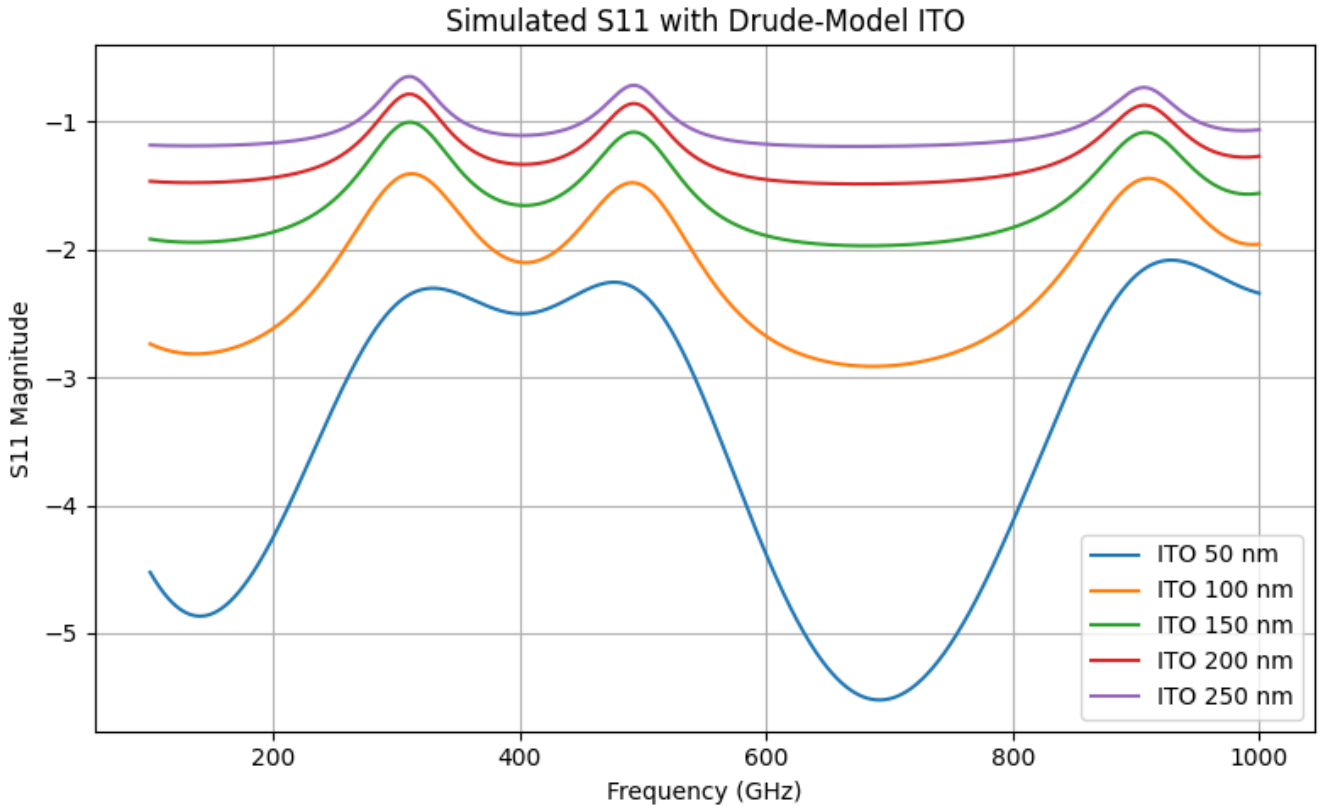

FIG. 10. Simulated S11 Magnitude (dB) vs. Frequency (GHz) for determining optimal deposition thickness.

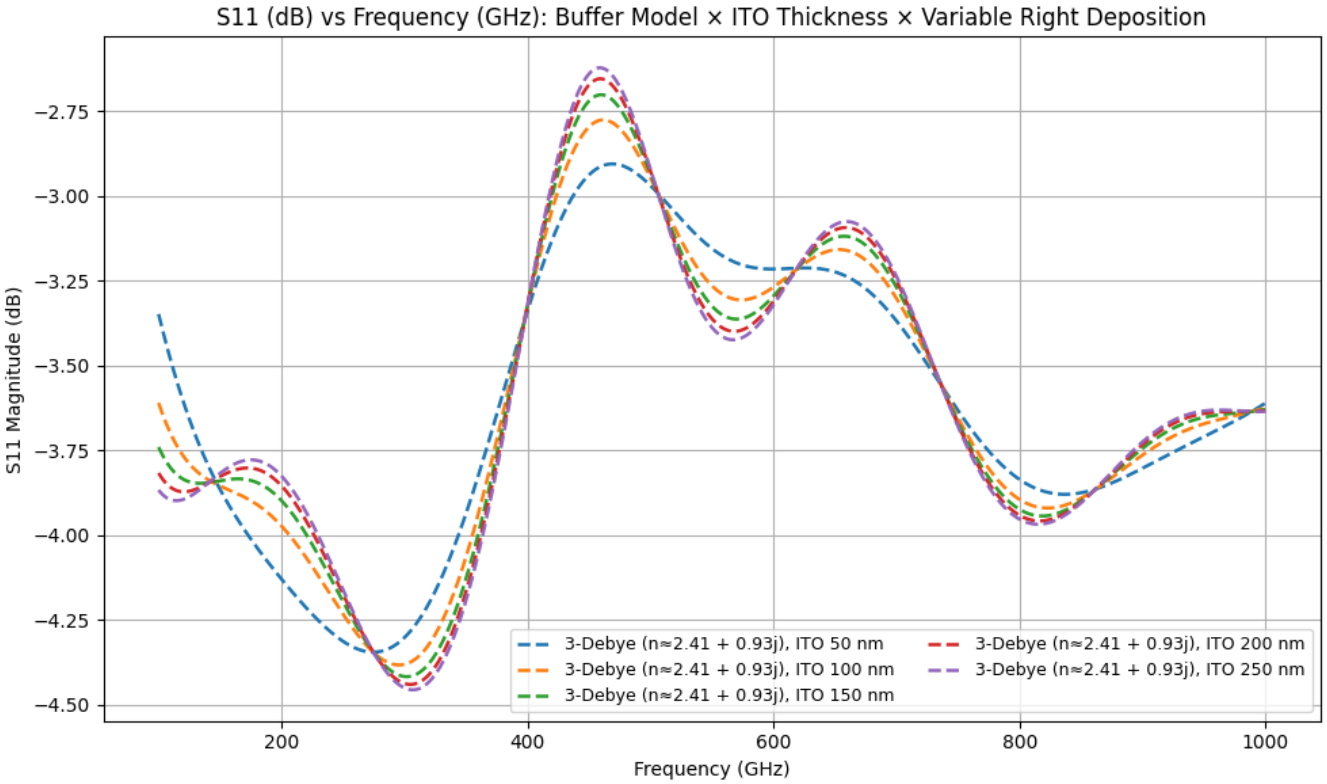

FIG. 11. Simulated S11 Magnitude (dB) vs. Frequency (GHz) for determining optimal deposition thickness with the left side held constant at 50 nm, and the right side variable.

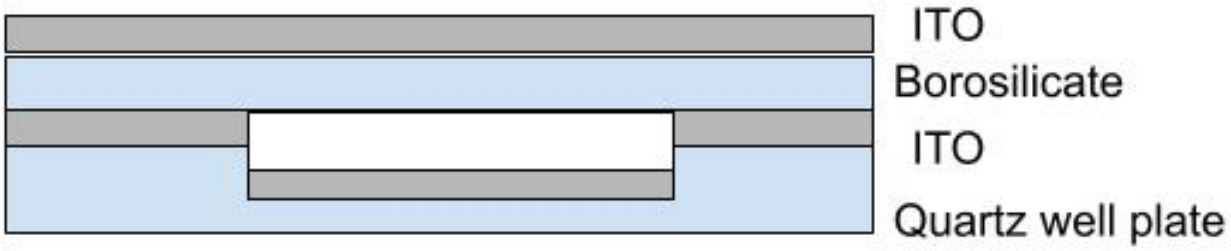

FIG. 12. Well-plate geometry as potential solution to enable resonance at 240 GHz. Credit:Nick Agladze